Assimilation for skin SST in the NASA GEOS atmospheric data assimilation system

Santha Akella[a,b]*, Ricardo Todling[a] and Max Suarez[a,c]

[a]*Global Modeling and Assimilation Office, NASA GSFC, Greenbelt, MD*

[b]*Science Systems and Applications, Inc., Lanham, MD*

[c]*Universities Space Research Association, GESTAR, Columbia, MD*

*Correspondence to: Code 610.1, NASA Goddard Space Flight Center, Greenbelt, MD 20771. E-mail: santha.akella@nasa.gov

The present article describes the sea surface temperature (SST) developments implemented in the Goddard Earth Observing System, Version 5 (GEOS-5) Atmospheric Data Assimilation System (ADAS). These are enhancements that contribute to the development of an atmosphere-ocean coupled data assimilation system using GEOS. In the current quasi-operational GEOS-ADAS, the SST is a boundary condition prescribed based on the OSTIA product, therefore SST and skin SST (Ts) are identical.

This work modifies the GEOS-ADAS Ts by modeling and assimilating near sea surface sensitive satellite infrared (IR) observations. The atmosphere-ocean interface layer of the GEOS atmospheric general circulation model (AGCM) is updated to include near surface diurnal warming and cool-skin effects. The GEOS analysis system is also updated to directly assimilate SST-relevant Advanced Very High Resolution Radiometer (AVHRR) radiance observations.

Data assimilation experiments designed to evaluate the Ts modification in GEOS-ADAS show improvements in the assimilation of radiance observations that extends beyond the thermal IR bands of AVHRR. In particular, many channels of hyperspectral sensors, such as those of the Atmospheric Infrared Sounder (AIRS), and Infrared Atmospheric Sounding Interferometer (IASI) are also better assimilated. We also obtained improved fit to withheld, in-situ buoy measurement of near-surface SST. Evaluation of forecast skill scores show marginal to neutral benefit from the modified Ts.

Key Words: SST; Diurnal Warming; AVHRR; Coupled Data Assimilation; NWP

Received . . .

1. Introduction

Skin sea surface temperature (SST) is essential for atmospheric data assimilation system (ADAS) because it is used to specify the lower boundary condition over the oceans. The analysis needs it for direct assimilation of satellite radiance observations, and the atmospheric general circulation model (AGCM) uses it to calculate important variables such as air temperature and air-sea fluxes.

The Skin SST in the Goddard Earth Observing System (GEOS) ADAS (Rienecker *et al.* 2011; Bosilovich *et al.* 2015) is specified based on already existing *daily* SST data products (Reynolds *et al.* 2002, 2007; Donlon *et al.* 2012). However, the near surface temperature is complex and highly variable within the day (Saunders 1967; Soloviev and Lukas 1997; Fairall *et al.* 1996; Webster *et al.* 1996; Ward 2006; Gentemann and Minnett 2008). Daytime solar heating in calm wind conditions leads to the formation of a diurnal warm layer and close to the air-sea interface there is typically a cool skin layer (see Gentemann and Minnett (2008) and references therein). Radiometric (infrared and microwave) measurements and in-situ buoys close to the sea surface have the capability to observe these changes (Donlon *et al.* 2002, 2007).

Prognostic models to simulate daily variation in skin SST have been implemented in the European Center for Medium-Range Weather Forecasts (ECMWF)-AGCM by Beljaars (1997); Zeng and Beljaars (2005); Takaya *et al.* (2010a). The Zeng and Beljaars (2005) model has been used by Brunke *et al.* (2008) in the Community Atmosphere Model version 3.1 (CAM3.1). Results from these models indicate that they can realistically simulate the near surface observed temperature variations (Takaya *et al.* 2010a), and also impact the model mean climatologies of precipitation, outgoing longwave radiation (OLR), latent and sensible heat fluxes (Brunke *et al.* 2008). In addition to these prognostic models, several diagnostic models (Fairall *et al.* 1996; Gentemann *et al.* 2009; Kawai and Wada 2007), and statistical models (Gentemann *et al.* 2003; Filipiak *et al.* 2010) have also been proposed. Bellenger and Duvel (2009) provide a discussion of the main differences between prognostic (e.g., Zeng and Beljaars (2005)) and diagnostic (Fairall *et al.* 1996) models.

In the context of data assimilation (DA) While and Martin (2013) tested a prototype system for producing near real time global analysis of diurnal SST using the Takaya *et al.* (2010a) (hereafter TBBJ10) model. They sampled a TBBJ10 model generated trajectory to obtain synthetic observations of a diurnally varying skin SST. Those observations were then assimilated using the same model in an attempt to recover the true initial state of the model, net heat flux and wind speed at every time step. Their experiments showed that they could improve the fit to the true state (compared to first guess) and also recover the initial model state and heat fluxes, but not the wind speed. One of their conclusions was that accurate specification of errors in forcing fields (heat fluxes and winds) and observations (of SST) are very important for a diurnal analysis of the global SST field. McLay *et al.* (2012) also implemented a version of the TBBJ10 model, without a cool skin layer in the Navy Operational Global Atmospheric Prediction System (NOGAPS). They obtained an improvement in precipitation (midday peak value and daily accumulation), and statistically significant differences in latent, sensible heat fluxes, OLR, 2m air temperature, etc. Overall, the diurnal skin SST provided improved forecasts in the tropics, with lower impact in mid-latitudes.

The objective of this article is to directly estimate skin SST using satellite radiance observations and the prognostic diurnal warming model of TBBJ10 and diagnostic cool skin layer model of Fairall *et al.* (1996) (now onwards F96) in the context of the NASA- GEOS version-5 ADAS (Rienecker *et al.* 2008; Bosilovich *et al.* 2015). Accurate interfacial states such as the skin SST (Curry *et al.* 2004) play an important role in a atmosphere-ocean coupled data assimilation (CDA) system (Dee *et al.* 2014; Lea *et al.* 2015; Laloyaux *et al.* 2016a,b); see Brassington *et al.* (2015) for a recent summary of the development of CDA systems at various operational centers. This article documents some of the preliminary steps that have been taken in the ADAS of the NASA Global Modeling and Assimilation Office (GMAO) to enhance the coupling between the atmosphere and ocean DA systems in preparation for an integrated earth system analysis (IESA).

The SST and sea ice concentration in the quasi-operational GEOS-5 ADAS come from the Operational Sea Surface Temperature and Ice Analysis system (OSTIA, Donlon *et al.*

(2012)) as lower boundary conditions. We made the following changes to the treatment of the SST in the ADAS. Since the OSTIA SST is an estimate of foundation SST, it does not contain diurnal variability, therefore we incorporated the TBBJ10 and F96 models into the AGCM to generate additional background (or, first guess) fields that are relevant to the diurnal variation of skin SST besides the already available upper air fields required to perform an atmospheric analysis. The atmospheric analysis is carried out using the Gridpoint Statistical Interpolation (GSI) (Kleist *et al.* 2009a,b) and it has been modified to analyze skin SST along with its upper air analysis. Taking advantage of the extensive use of the Advanced Very High Resolution Radiometer (AVHRR) measurements for SST retrievals (Reynolds *et al.* 2007; May *et al.* 1998), we included AVHRR brightness temperature observations from both NOAA-18 and Metop-A satellites to the ADAS observing system. All satellite observations are directly assimilated by GSI using the community radiative transfer model (CRTM*) (Han *et al.* 2006; Chen *et al.* 2010); the interface between the GSI and CRTM has also been modified to account for the skin SST. We emphasize that with these changes in place, the CRTM uses a diurnally varying skin SST to simulate brightness temperatures (for all satellite sensors/channels), as opposed to using the daily OSTIA SST field. Finally, the analysis increment (includes the increment in skin SST) is then used to force the AGCM through the incremental analysis update (IAU) approach (Bloom *et al.* 1996).

Layout of this article is as following. Section 2 provides a description of the modifications to the GEOS-AGCM to obtain a diurnally varying skin SST. We include some account of the turbidity of water due to biological activity, because it affects the net shortwave radiation that is absorbed within the near-surface ocean; however, we parameterized the impact of Langmuir circulation. Section 3 details the interconnectivity of the AGCM and GSI analysis (observing system and CTRM) that is involved in calculating an estimate for skin SST. Section 4 presents the experimental set up. Section 5 shows results with and without the modified SST, including and excluding the AVHRR observations. Corresponding changes in the performance of the numerical weather prediction (NWP) system are presented in section 6. Finally, in section 7, we summarize our results, followed with a brief outline of current work.

2. Skin SST model in the GEOS-AGCM

In the GEOS-AGCM, net surface heat flux over the ocean served as a diagnostic variable (Molod *et al.* 2012) and the skin SST (denoted by T_s) is set equal to the daily OSTIA SST. This section describes changes made to this formulation to obtain a diurnally varying T_s. Following F96, we calculate the near sea surface temperature at any depth

$$T(z) = T_d - \Delta T_c + \Delta T_w(z), \tag{1}$$

where T_d is the OSTIA SST, ΔT_w and ΔT_c denote diurnal warming and cool-skin temperature changes respectively, and are described below; T_s is simply $T(z=0)$.

2.1. *Cool skin*

Up to a few millimeters below the air-sea interface, heat loss occurs due to the exchange of net longwave, sensible and latent fluxes. This negative heat flux dominates the absorbed shortwave radiation resulting in the formation of a cool skin layer (F96; Saunders (1967); Curry *et al.* (2004)). We follow F96 to diagnostically calculate the thickness and temperature drop, ΔT_c, within this cool layer,

$$\Delta T_c = \frac{\delta}{\rho_w \, c_w \, k_w} Q^c_{net}, \tag{2}$$

where $\rho_w \, c_w$ and k_w denote density, heat capacity and thermal conductivity of sea water respectively. δ is the thickness of this layer,

$$\delta = \frac{\lambda \, \nu_w}{u_{*,w}}, \tag{3}$$

ν_w is the kinematic viscosity, friction velocity over water is given by $u_{*,w} = u_{*,a}\sqrt{\rho_a/\rho_w}$; $u_{*,a}$ is the atmosphere friction velocity and ρ_a is air density. The net heat flux in this cool layer, Q^c_{net}, is give by

$$Q^c_{net} = (H_s + H_l - LW_{net}) - f_c \, SW^s_{net} \tag{4}$$

*Version 2.1.3 is used in this work

where H_s, H_l, LW_{net}, and SW^s_{net} denote the surface sensible, latent, net longwave and shortwave heat fluxes respectively; as in F96 heat fluxes are positive downward. Only a fraction (f_c) of SW^s_{net} is absorbed in the cool-skin layer; f_c and λ are calculated as in F96. Also following F96, we assume a linear variation of temperature within this layer, $T(z) = T_\delta - \Delta T_c\ (1 - \frac{z}{\delta}),\ 0 \leq z \leq \delta$. T_δ is the temperature at depth $z = \delta$, i.e., at the top (bottom) of the warm (cool) layer, is explained below.

2.2. *Diurnal warming*

Following the single column prognostic model of TBBJ10, we calculate the diurnal warming as

$$\frac{\partial(T_\delta - T_d)}{\partial t} = \frac{(\mu_s + 1)Q^w_{net}}{\mu_s\, \rho_w\, c_w\, d} - \frac{(\mu_s + 1)\, \kappa\, u_{*,w}\, f(La)}{d\, \phi_h(\zeta)}\, (T_\delta - T_d), \tag{5}$$

where d denotes a fixed depth below the cool layer and $\kappa = 0.4$ is the von Kármán constant; $La = \sqrt{\frac{u_{*,w}}{u_s}}$, is the Langmuir number, u_s is the surface Stokes velocity, and $f(La) = La^{-2/3}$. The stability parameter, $\zeta = z/L$ involves the Obukhov length, is given by $L = \frac{\rho_w\, c_w\, u^3_{*,w}}{\kappa\, g\, \alpha_w\, Q^w_{net}}$. The similarity function is defined as

$$\phi_h(\zeta) = \begin{cases} 1 + \frac{5\zeta + 4\zeta^2}{1 + 3\zeta + 0.25\zeta^2} & \text{if } \zeta \geq 0, \\ (1 - 16\zeta)^{-1/2} & \text{if } \zeta < 0. \end{cases} \tag{6}$$

where μ_s is an empirical parameter (≤ 1) whose small values lead to sharper near-surface peaking of the temperature profile within the warm layer ($\delta \leq z \leq d$): $T(z) = T_\delta - \left(\frac{z-\delta}{d-\delta}\right)^{\mu_s} (T_\delta - T_d)$, $\Delta T_w(z) = T(z) - T_d$.

Our implementation of the TBBJ10 model differs in the following fashion. Due to the absence of a wave model in the GEOS, we set the surface Stokes velocity $u_s = 1\mathtt{cm/s}$ globally. This value was obtained based on trial and error and off-line matching of model simulations with buoy-measured temperature time series. For this reason, we do not adjust the second term on the right hand side of (5) as done by TBBJ10 and Zeng and Beljaars (2005) (hereafter ZB05) to obtain a slow decay of ΔT_w after sunset (when $SW^s_{net} \approx 0$). In the future, we plan to revisit these choices in coordination with the implementation of a wave model to simulate the relaxation of T_δ to T_d.

The net heat flux in the warm layer, Q^w_{net}, is given by

$$Q^w_{net} = SW^w_{net} + (LW_{net} - H_s - H_l), \tag{7}$$

where $SW^w_{net} = SW^s_{net} - SW_{PEN}$, is the net shortwave radiation absorbed in the warm layer. ZB05 and TBBJ10 used the three-band absorption profile of Soloviev (1982) to obtain the penetrating shortwave radiation, SW_{PEN} given by

$$\frac{SW_{PEN}(z)}{SW^s_{net}} = \sum_{i=1}^{N=3} a_i\, \exp\left(-z\, b_i\right), \tag{8}$$

where $z = d$; the coefficients a_i and b_i are as in ZB05. A modified version of the nine-band model of Paulson and Simpson (1981) was used by Gentemann *et al.* (2009) and While and Martin (2013). Besides the obvious differences in the number of terms ($N = 3$ or 9) and values of coefficients (a_i, b_i), the nine-band model differs from the three-banded model because it also includes contribution from the solar zenith angle in b_i (Gentemann *et al.* 2009).

Ohlmann and Siegel (2000) and Wick *et al.* (2005) suggested that SW_{PEN} is sensitive to the upper-ocean chlorophyll concentration, solar zenith angle and cloud cover. Ohlmann (2003) suggested a chlorophyll dependent, parameterized shortwave absorption model based on results from an ocean radiative transfer model which considered absorption in $250 - 2500$ nm wavelength range. In the present work, we make an effort to compare the impact of three-band (Soloviev 1982) and nine-band (Gentemann *et al.* 2009) shortwave absorption models in our implementation of TBBJ10 diurnal warming by simply changing the way we calculate SW_{PEN}. We also tried to include the impact of chlorophyll, but unlike Ohlmann (2003) we consider absorption in the visible and ultraviolet (UV) wavelength range in a simple fashion,

$$\begin{aligned} SW_{PEN}(z) \quad = \quad & \left[(1 - \alpha_{VR})DR_{UV} + (1 - \alpha_{VF})DF_{UV}\right]\beta_{UV} + \\ & \left[(1 - \alpha_{VR})DR_{PAR} + (1 - \alpha_{VF})DF_{PAR}\right]\beta_{PAR} \end{aligned} \tag{9}$$

where $\beta_{UV} = \exp(-z\, K_{UV})$ and $\beta_{PAR} = \exp(-z\, K_{PAR})$, α_{VR} and α_{VF} denote surface direct beam and diffuse albedos over water, respectively. The surface downwelling direct and

diffuse fluxes in the UV are given by DR_{UV} and DF_{UV} respectively. DR_{PAR} and DF_{PAR} denote the direct and diffuse photosynthetically active radiation (PAR) fluxes, respectively (for details regarding these fluxes in the GEOS-AGCM, please see Rienecker *et al.* (2008)). The extinction coefficient K_{UV} is set to a constant value of $0.09\,\mathrm{m}^{-1}$, whereas K_{PAR} is specified based on a climatology of chlorophyll concentration derived from SeaWiFs and is the same as that used in the GEOS atmosphere-ocean coupled model (Vernieres *et al.* 2012; Ham *et al.* 2014), see Figure 1. Typically higher concentrations of chlorophyll are found near coastlines and in regions where upwelling of cold water takes place. Turbidity of water is higher in these regions, leading to larger K_{PAR}, consequently shortwave radiation does not penetrate deep into the water column (for details, please see Morel *et al.* (2007)). Based on (9) high values of K_{PAR} imply lower β_{PAR} and SW_{PEN}, hence larger SW^{w}_{net}, i.e., more shortwave radiation in the warm layer. This inverse relationship between K_{PAR} and SW^{w}_{net} can be also noticed at locations with less chlorophyll concentrations, which have lower values of K_{PAR}, therefore, sunlight penetrates into deeper ocean.

In the skin SST model we set depth $d = 2\,\mathrm{m}$, and followed the procedure described by ZB05 for the parameter μ_s and set it to 0.2. As in ZB05 and TBBJ10, we integrate (5) in time, using an implicit scheme to predict T_δ, and then use (2) and (1) to calculate $T(z)$.

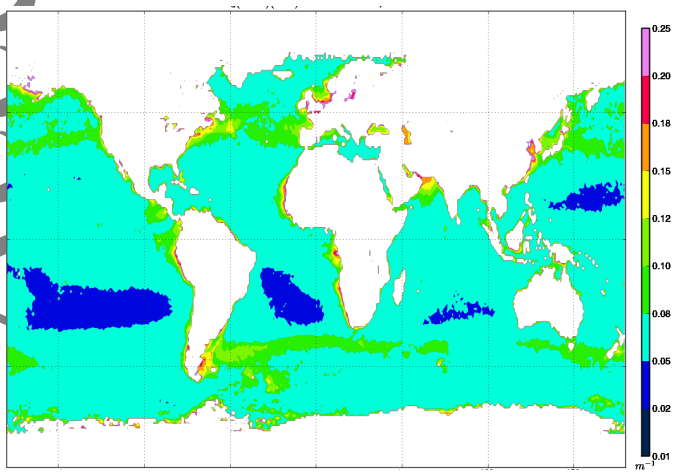

Figure 1. Climatological downward diffuse attenuation coefficient for the photosynthetically available radiation, K_{PAR} (m^{-1}) for the month of April. Values over land and sea ice have been masked and are not used in open ocean computations.

Atmospheric processes induce a two-way feedback between aerosols (particularly, dust) and skin SST (May *et al.* 1992; Merchant *et al.* 2006). Here we make no attempt to diagnose those mechanisms; for now, we leave this topic to future work. We use the Goddard chemistry, aerosol, radiation, and transport (GOCART) model, active in GEOS-AGCM (Rienecker *et al.* 2008), and therefore aerosols impact the skin SST simulated in the model.

3. Analysis of skin SST using GEOS-ADAS

Using the first guess, or *background* fields generated by the GEOS-AGCM, we analyze a wide variety of satellite and in situ observations in the framework of GEOS-ADAS (Rienecker *et al.* 2008, 2011). The atmospheric analysis uses the three-dimensional variational (3D-Var), first-guess-at-the-appropriate-time (FGAT) flavor of GSI (Kleist *et al.* 2009a,b). GSI analysis control vector includes T_s, surface pressure and also their upper air fields. The analysis increment: T_s^{inc} (difference between analyzed and background T_s) $T_s^{ana} - T_s^{bkg}$, was not taken into account by the ensuing AGCM integration (Derber and Wu 1998; Rienecker *et al.* 2008). To estimate T_s, following changes were made to the GEOS-ADAS.

3.1. *Observation minus background computation and background error*

With the inclusion of the skin SST model in the AGCM (section 2) additional (two dimensional) fields (depths: δ and d, temperatures: T_δ and T_d and the temperature drop due to the cool skin layer: ΔT_c) are available to the GSI. FGAT for these additional fields at the observation time, t_k and location (latitude, longitude and depth: z_{ob}) are obtained in the following steps, (i) temporally (linearly) interpolate above fields to t_k, (ii) spatially interpolate them to the observation spatial location using bilinear interpolation, and (iii) calculate the temperature at the observation depth following the temperature profile in the cool-skin (section 2.1) and diurnal warm (section 2.2) layers according to,

$$T(z_{ob}) = \begin{cases} T_\delta - \Delta T_c \left(1 - \frac{z_{ob}}{\delta}\right) & \text{if } 0 \le z_{ob} \le \delta \ (\textbf{Cool Layer}), \\ T_\delta - \left(\frac{z_{ob}-\delta}{d-\delta}\right)^{\mu_s} (T_\delta - T_d) & \text{if } \delta < z_{ob} \le d \ (\textbf{Warm Layer}). \end{cases} \quad (10)$$

This temperature profile $T(z_{ob})$ is used as the first guess or background field to calculate observation minus background (OMB).

Observations that are taken close to the sea surface ($z_{ob} \approx 0$) are influenced by diurnal warming and cool skin and $T(z_{ob}) \approx T_s$. Whereas observations taken below the cool layer ($z_{ob} > \delta$) feel the presence of a warm layer only (Donlon *et al.* 2007).

For in situ measurements, z_{ob} is the measurement depth; for the satellite observations, it is non-trivial and it is related to the wavelength of the electromagnetic radiation (Wieliczka *et al.* 1989), and scan angle (C. Gentemann, personal communication, 2012). Following Donlon *et al.* (2007) we set the following values for z_{ob}

$$z_{ob} = \begin{cases} 15\,\mu\mathrm{m} & \text{all infrared sensors,} \\ 1.25\,\mathrm{mm} & \text{all microwave sensors.} \end{cases} \tag{11}$$

A more precise (wavelength dependent) computation of the z_{ob} for infrared (IR) and microwave (MW) sensors is beyond the scope of this study.

Computation of the OMB residuals for in situ observations is trivial. Whereas for satellite radiance observations, we first calculate $T(z_{ob})$ using (11) and (10). This temperature at z_{ob} and upper-air atmospheric fields are then used by the CRTM to simulate a brightness temperature (T_b) and hence obtain the OMB for any satellite/sensor; the CRTM also returns the sensitivity $\partial T_b/\partial T_z$. However, since the analysis control variable is T_s, we need the Jacobian of the brightness temperature with respect to T_s : $\partial T_b/\partial T_s$ for the linearized observation operator needed in the 3D-Var minimization. This is obtained through the chain rule, $\partial T_b/\partial T_z = (\partial T_b/\partial T_s)\,(\partial T_s/\partial T_z)$, where we use a simple approximation for the Jacobian, $\partial T_s/\partial T_z = 1$. This is reasonable for IR observations because we assume in (11) that the penetration depth is $15\,\mu\mathrm{m}$ (very close to the air-sea interface, $T(z = 15\,\mu\mathrm{m}) \approx T_s$). But it is not accurate for MW observations, because $z_{ob} \sim O(1\,mm)$. Since this approximation for $\partial T_s/\partial T_z$ is not realistic for MW observations, it will require further investigation in future work.

Regarding the background error for T_s, we use the same covariance structure as in Derber and Wu (1998) and follow their procedure in assuming it to be independent from other analysis control variables; the correlation length scales and standard deviation are shown in Figure 2. As noted in Derber and Wu (1998), the correlation length scales can be improved upon to account for the short correlation length scales that are typically seen for oceanic variables such as the SST (Donlon *et al.* 2012), this topic is part of our current work (section 7).

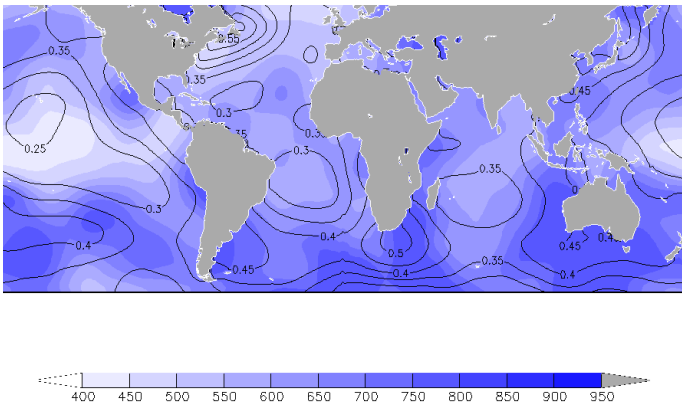

Figure 2. T_s background error correlation length scales is shaded (in km) and standard deviation is contoured with 0.05^oC interval between $\pm 60^o$ latitudes. Values of standard deviation range from zero over sea ice-covered regions to about 0.7^oC in regions of high variability, such as the Gulf stream and Kuroshio current regions; correlation length scales vary between 400 and 900 km; land has been masked out.

3.2. *SST relevant additional observations*

SST relevant observations are available from in situ platforms (ships, moored and drifting buoys). Though they directly measure temperature, they have limited spatial coverage and temporal frequency. Also, they do not measure within microns (or even millimeters) of the air-sea interface (Donlon *et al.* 2002). The measurements that are most representative of the skin SST are made by drifting buoys (Lumpkin and Pazos 2007). They record hourly temperature at approximately 20cm depth, and therefore provide most temporally continuous observations of the SST, *close* to the air-sea interface. Unfortunately, there is no uniform global coverage, and there are significant gaps at high latitudes. Our immediate goal is to focus on the skin SST, so we focus on the assimilation of satellite observations, and withhold in situ SST observations to passively monitor the OMB to diagnose any systematic biases.

Satellite measurements in the IR ($3.7 - 12\,\mu\mathrm{m}$ wavelengths) and MW ($6 - 11\mathrm{GHz}$ frequency) provide long term, continuous measurements of near-surface temperature (Hosoda 2010; Castro *et al.* 2008; Donlon *et al.* 2007). In GEOS-ADAS, analysis

of MW observations in the SST relevant frequency range is currently under development, and we do not consider them in this work. AVHRR observations in the IR have been extensively used for SST retrievals (May *et al.* 1998; Reynolds *et al.* 2007). Taking advantage of their availability from the Environmental Modeling Center (EMC), we added AVHRR T_b observations from both NOAA-18 and Metop-A satellites to the GEOS-ADAS observing system. Level 1B, global area coverage (GAC) ocean only data was obtained at a resolution of about $4\ \mathrm{km}^2$, it includes a cloud mask and it has information in three IR window channels (3B centered around $3.7\,\mu\mathrm{m}$, channels 4 and 5 approximately around 11 and $12\,\mu\mathrm{m}$ wavelengths respectively). Due to solar contamination (Liang *et al.* 2009) channel 3B (henceforth referred as channel 3) daytime data is not used. The procedure for reading, spatial thinning, observational scoring and quality control (QC) of the data follows the treatment for any IR sounding observations currently handled by GSI. Abundant precaution is taken to detect clouds and to reject observations that are deemed to be affected by them (Akella *et al.* 2016). Channel 3 is most sensitive to skin temperature, therefore it has the most potential to drive the T_s analysis increment. However, similar wavelength IR channels (on other sensors) are currently inactive (i.e., not assimilated) in the GEOS-ADAS and in general, it is challenging to assimilate such observations because of the complexities in radiative transfer modeling at such wavelengths (Chen *et al.* 2012). Nevertheless we have attempted to conservatively assimilate observations from this channel (as already mentioned, only at local nighttime), and by having a smaller contribution to the 3D-Var cost function (and its gradient), achieved by down-weighting the observational error variance computed using the GSI QC procedure (Derber and Wu 1998; Akella *et al.* 2016). Approximately 36 thousand observations are available within a 6 hr analysis window (in all 3 AVHRR channels, and on both NOAA-18 and Metop-A satellites) after thinning and scoring, of which about 65% observations are rejected by QC procedure.

Due to errors in the satellite instruments and their calibration, and also systematic errors in radiative transfer models, satellite radiance data assimilation involves usage of a variational bias correction (VarBC) procedure (Derber and Wu 1998; Dee and Uppala 2009; Eyre 2016). As all other satellite observations, the AVHRR observations are also bias corrected using the VarBC. The observational error standard deviation, σ_o is set to $0.60, 0.68,$ and 0.72^oK for channels 3, 4 and 5 respectively. These values are chosen such that the AVHRR σ_o is lower than that specified for other surface sensitive IR observations.

3.3. *Application of skin SST analysis increment*

Using all the observations (regularly analyzed by GEOS-ADAS, plus AVHRR) and background fields (section 3.1), we obtain analyzed fields (T_s included). All analysis increments are applied to the GEOS-AGCM using the IAU approach (Bloom *et al.* 1996). We apply the increments of upper-air and surface pressure fields over all surface types (ice, land, water), but the T_s increment is applied only over open ocean (where the fraction of water is equal to 1).

4. Experimental setup

The following additions to GEOS-ADAS:

(a) modeling of diurnal variations in SST in GEOS-AGCM,
(b) addition of AVHRR observations to the analysis system,
(c) usage of the analysis increment in skin SST by the AGCM,

are evaluated with the aid of following experiments.

(i) **CTL** mimics the current quasi-operational configuration of GEOS-ADAS with a 3D-Var DA. It uses OSTIA SST for skin SST and AVHRR observations are not assimilated. The analysis increment in T_s is ignored in the AGCM integrations.

(ii) **AVH** is like the CTL, but it adds AVHRR data from NOAA-18 and Metop-A to the analysis system. Here the model continues to ignore the T_s analysis increment.

(iii) **tSkin** is similar to the CTL and does not assimilate AVHRR data. But it has the skin SST model turned on. Therefore the model produced diurnal warming and cool skin are used to compute T_s, which is then used by the CRTM. The Skin SST model used the K_{PAR} (9) for computation of the penetrating shortwave radiation. The T_s analysis increment is ignored by the model.

(iv) **Assim_Kpar** uses the skin SST model, configured as in tSkin. In addition it assimilates the AVHRR observations. The CRTM uses $T(z_{ob})$ (given by (10)) with the values of z_{ob} for all IR and MW instruments given in (11). Here the analysis increment in T_s is used by the AGCM through IAU. This experiment, therefore, implements all items (a)-(c) above.

(v) **Assim_Sol82** is like Assim_Kpar, but uses the three-band Soloviev (1982) shortwave absorption model instead of the K_{PAR} based SW_{PEN}.

(vi) **Assim_PS81** is like Assim_Kpar, but uses the modified version of Paulson and Simpson (1981) nine-band shortwave absorption model from Gentemann *et al.* (2009).

A summary of the experimental setup is given in Table 1, we will refer to experiments: **(iv)- (vi)** as *T_s assimilation experiments*.

Using initial conditions from the above ADAS experiments, we also performed NWP experiments (see section 6).

The experiments are configured at about $\frac{1}{2}^o$ (576×361) horizontal resolution on a cube sphere (C180) grid (Putman and Lin 2007), with 72 vertical levels (Rienecker *et al.* 2008), and a time step of 450 seconds. All experiments are started with the same initial conditions, with 15-days (16- 31 March 2012) of spin-up; all evaluations are for April 2012[†].

5. Results and discussion

We start with a description of the results from the skin SST model, focussing on the cool skin and diurnal warming. Thereafter proceed to evaluate the analysis of observations via direct examination of observations minus background (OMB) and observation minus analysis (OMA), including in situ SST withheld observations (section 5.2). We compare the T_s analysis increments in (section 5.3). As noted before, we do not apply the T_s analysis increment (T_s^{inc}) over land and sea ice (section 3.3), thus we focus on the open ocean results.

5.1. *Skin SST*

The skin SST model is used in the tSkin and T_s *assimilation experiments*. The April 2012 monthly mean temperature drop

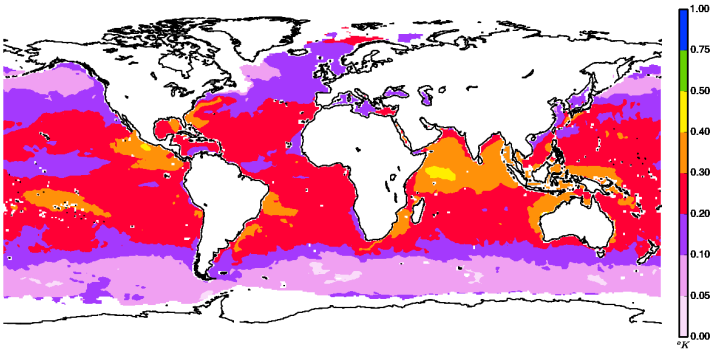

Figure 3. April 2012 monthly mean of the temperature drop ΔT_c (^oK) due to the cool-skin layer for the tSkin experiment. Land and sea ice have been masked.

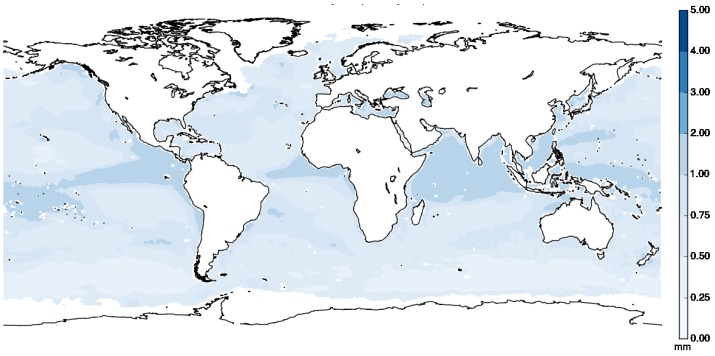

Figure 4. Same as in Fig. 3 but for the depth of the cool-skin layer δ (mm).

(ΔT_c) due to the cool-skin layer, for tSkin experiment is shown in Fig. 3. ΔT_c peaks to about $0.4 - 0.5^oK$ in light wind conditions (in tropics) and decreases to around 0.05^oK with increasing wind speed (for instance in the Southern Ocean), similar results were also reported by Saunders (1967) and F96. The mean thickness of the cool layer (δ) is shown in Fig. 4, and it is inversely related to friction velocity over water ($u_{*,w}$, not shown) via (3).

Based on (2), we also expect a direct correlation between ΔT_c and the net heat flux in the cool layer (Q^c_{net}). During daytime we obtained a decrease of about $0.1^o - 0.2^oK$ in ΔT_c, due to (4), which includes a negative contribution from the net surface shortwave radiation (SW^s_{net}). Regions of low wind speed, for instance the tropical eastern Pacific and Indian Oceans, show largest daily variability, similar variation was noted by F96. We obtain similar values for cool skin layer fields ($\Delta T_c, \delta$) in the T_s *assimilation experiments*.

The combination of diurnal warming (ΔT_w) and cool skin impacts the T_s (1); difference between T_s and OSTIA SST (T_d)

[†]AVHRR satellite bias correction coefficients (for both NOAA-18 and Metop-A) were spun up from zero values using low resolution experiments.

Table 1. Summary of experimental setup (details are given in section 4)

Exp. Name	skin SST model	Shortwave penetration	T_s used by CRTM	AVHRR obs	T_s Analysis Increment
CTL	off	N/A	OSTIA SST	not used	not used
AVH	off	N/A	OSTIA SST	analyzed	not used
tSkin	on	K_{PAR} based	skin SST (Eq.(1))	not used	not used
Assim_Kpar	on	K_{PAR} based	$T(z_{ob})$ (Eq.(10))	analyzed	used
Assim_Sol82	on	Soloviev (1982)	$T(z_{ob})$ (Eq.(10))	analyzed	used
Assim_PS81	on	modified Paulson and Simpson (1981)	$T(z_{ob})$ (Eq.(10))	analyzed	used

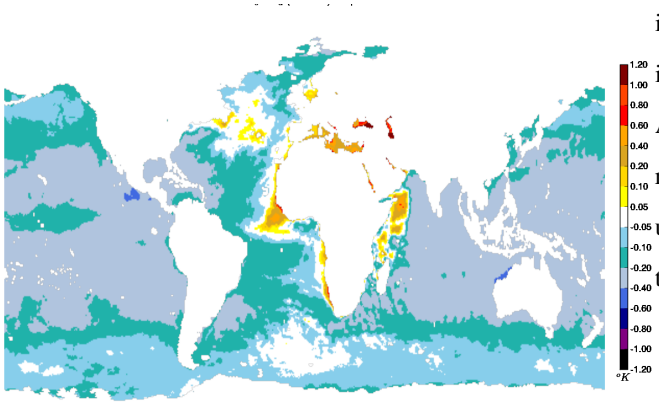

Figure 5. April 2012 monthly mean difference between skin and OSTIA SSTs (^oK) for the tSkin experiment at 12 UTC.

is shown in Fig. 5 for the tSkin experiment. Positive (negative) differences are related to the increase (decrease) due to the contribution from ΔT_w (ΔT_c). The diurnal warming is driven by insolation and modulated by winds (5). Tropical oceans (with low wind speed) have largest diurnal warming (as also reported by ZB05 and TBBJ10), for example, in the Indian Ocean (Somali basin in Fig. 5) we obtain ΔT_w around 2^oK. In the extratropics we obtain smaller diurnal warming than in the tropics due to the typical higher wind speeds and lesser insolation.

Figure 6 shows the difference in skin SST for the T_s *assimilation experiments* from tSkin experiment at 12UTC. We obtained an increase of up to 0.2^oK during afternoon- evening local times, larger differences are seen for the Assim_Sol82 and Assim_PS81 experiments. We attribute these changes to the following three reasons: (i) application of analysis increment in T_s (details follow in section 3.3), which was not applied in the tSkin experiment; (ii) tSkin and Assim_Kpar both used (9) for shortwave radiation penetration (SW_{PEN}), whereas the other two assimilation experiments use different shortwave absorption profiles (table 1); (iii) analysis of AVHRR observations (see section 5.2), not used in tSkin. The difference in the absorbed shortwave radiations is shown in Fig. 7. Difference between Assim_Kpar and tSkin is small and noisy, as shown in Fig. 7(b). Assim_Sol82 and Assim_PS81 have about $20W/m^2$ more net surface shortwave radiation (SW^s_{net}) than tSkin, which is perhaps the largest contributor to the differences in T_s, in Fig. 6(c, d). This result highlights the importance of SW_{PEN} in modeling diurnal warming.

The diurnal SST amplitude (DSA) metric has been used by TBBJ10 to compare their modifications to the ZB05 scheme; it has also been used by Bellenger and Duvel (2009) and McLay *et al.* (2012). At any given location, TBBJ10 defined DSA to be equal to T_s(max)- T_s(min) during 00 to 24 hours local mean time. They use hourly output between latitudes $= \pm 40^o$ for a period of 17 years and show average DSA as a function of averages of 10 m wind speed and insolation. TBBJ10 and Bellenger and Duvel (2009) also compared their results with empirical estimates based on Gentemann *et al.* (2003); see TBBJ10 for further details. In an attempt to validate our skin SST model results, we report the April 2012 averaged DSA as a function of 10 m wind speed and insolation, and between $\pm 60^o$ latitudes. This is shown in Fig. 8. Because of the relatively small sample size (only 1 month), our figure does not include insolation value of $350\,W/m^2$ and includes only one data points for up to $10\,ms^{-1}$ wind speed. All T_s *assimilation experiments* have larger DSA than the tSkin experiment (for most wind speeds and insolation), and the largest was obtained for the Assim_Kpar experiment, particularly at low wind speeds. The DSA for Assim_Kpar peaks to about 3^oK at $1m/s$ wind speed and $300\,W/m^2$ insolation, whereas in the case of TBBJ10 it was about 2.25^oK. Also the rate at which the DSA rises for low wind speed values seems to be too steep. Considering DSA as a function of insolation (right panel of Fig. 8), we obtain a sharper increase between $250 - 300\,W/m^2$ and, except for the

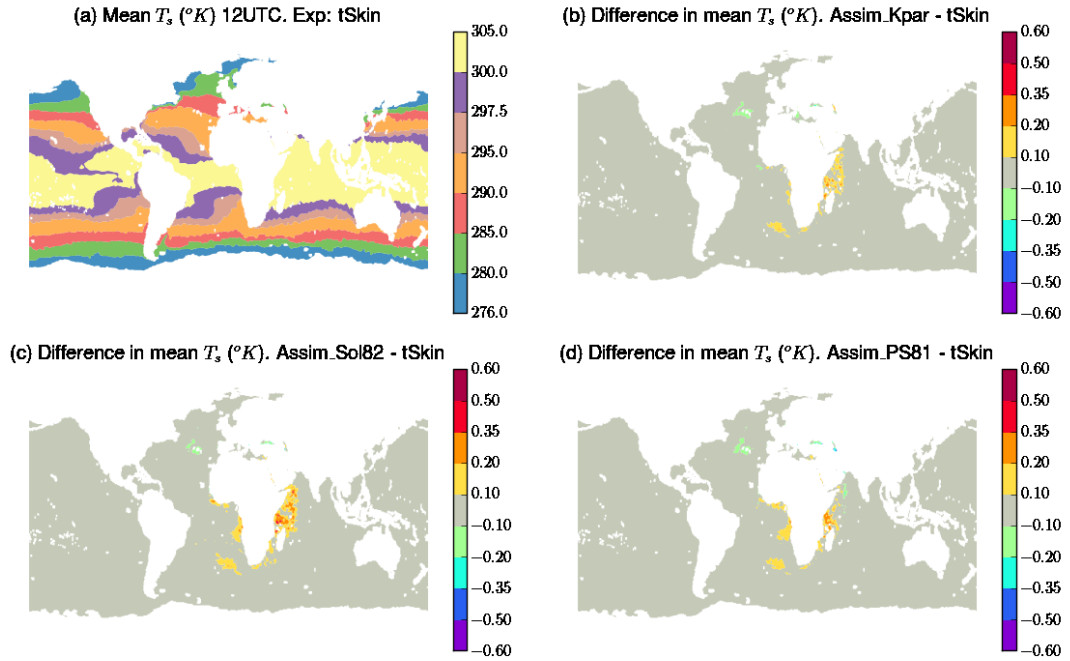

Figure 6. (a) Monthly mean of T_s for tSkin experiment at 12UTC. Panels (b)- (d) depict differences from other experiments.

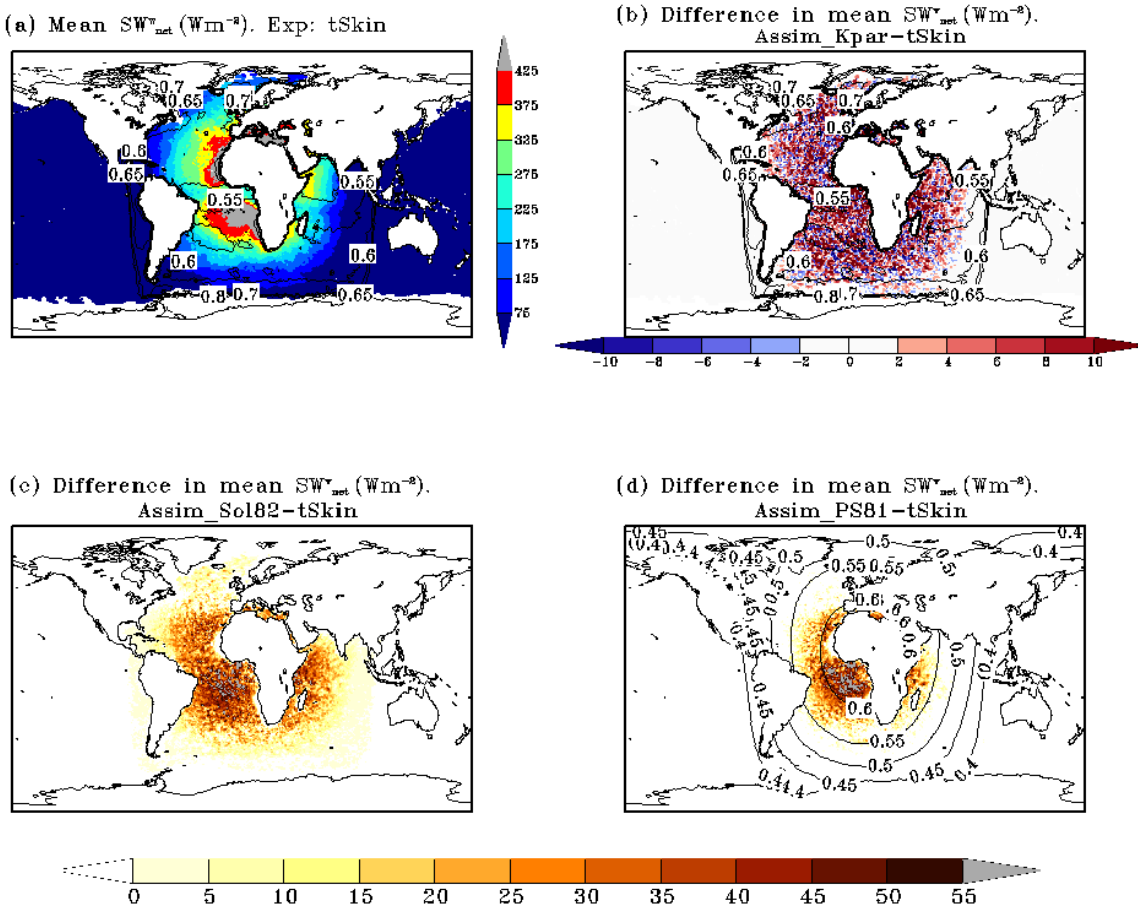

Figure 7. (shaded) Monthly mean of net shortwave radiation absorbed in the diurnal warm layer (SW^w_{net}) in W/m^2 at 12UTC. Contours depict the ratio: SW^w_{net}/SW^s_{net}. Contours are not shown in panel (c) for the Assim_Sol82 experiment because $SW^w_{net}/SW^s_{net} = 0.61$ when using the Soloviev (1982) absorption profile at $d = 2m$ depth.

$6m/s$ wind speed, our DSA values are larger than those obtained by TBBJ10[‡].

Spatial distribution of DSA and the difference among the experiments is shown in Fig. 9. Similar to the differences in T_s, shown in Fig. 6, T_s assimilation experiments have larger DSA

[‡] We do not include a comparison with Gentemann *et al.* (2003) empirical estimates, because it arrives at similar conclusions (C. Gentemann, personal communication, 2014).

than tSkin experiment, with peak difference (of about 0.5^oK) seen in the Indian ocean. As in the case of the differences in T_s, we attribute these differences in DSA to the same reasons (that is, application of the T_s analysis increment, differences in shortwave absorption and, usage of AVHRR observations). However, DSA of about 3^oK for low wind speeds and also high values in the Indian Ocean (the maximum DSA reported by TBBJ10 is about 2.5^oK) underscores the need to improve our similarity function, turbulent diffusivity (mixing due to surface waves). TBBJ10 also stressed the importance of the accuracy of the Langmuir number La, for diurnal warming calculation; comparison of their DSA with ZB05 shows that the similarity function and La can significantly impact the maximum DSA. As mentioned in section 2.2, we took a simple approach to calculate La which lead to a range of $f(La)$ between unity and roughly 1.6; values are comparable to the global constant value used by McLay *et al.* (2012) who also had no access to a wave model and set $f(La) = 1.4$ globally. Similar issues regarding validation of DSA have also been noted by Takaya *et al.* (2010b) and McLay *et al.* (2012). There are limitations to the validation of DSA (please see TBBJ10, sections 3.3 and 4), in section 5.2 we directly compare our near-surface temperature $T(z)$ with withheld in situ SST measurements.

5.2. *Background and analysis departures*

The GEOS-ADAS assimilates a wide variety of in situ (conventional) and satellite (polar orbiting and geostationary) observations. The majority of these data are brightness temperature (T_b) observations (Rienecker *et al.* 2008; Bosilovich *et al.* 2015). The overall impact on the analysis of conventional upper-air measured temperature, winds, moisture, and surface pressure for the experiments was minimal when compared to the CTL; change in fit to the observations (mean and standard deviation) is less than 1%. This is probably due to the fact that most of these observations are in the northern hemisphere, on land and are not directly impacted by the skin SST changes considered here.

Drifting buoys (section 3.2) measure near surface SST and are part of the in situ observations that are used in the generation of SST analyses, such as the OSTIA SST[§]. They have also been used by Castro *et al.* (2012) for validation of satellite SST data products; Kennedy *et al.* (2007) used them to create a climatology of diurnal warming. The GEOS-ADAS does not analyze these observations, but we obtained them from the NOAA/NESDIS iQuam, and used them to validate our near-surface temperature from the tSkin and T_s *assimilation experiments*. Using the highest level of quality controlled observations (Xu and Ignatov 2014), and measurement depth $z_{ob} = 20$ cm in (10), we calculate the fit of our background fields to these SST observations (using a different value for z_{ob}, say 25 cm did not affect evaluation). The basin averaged mean OMB is shown in Fig. 10. Based on the design of the OSTIA SST analysis (Donlon *et al.* 2012), observations that could have observed any diurnal warming would not have been analyzed, and if we assimilated them, we would have expected a mean OMB close to zero, hence no diurnal cycle in the OMB. However, since these observations were withheld, the only way we could change our fit to the data was with our skin SST model produced diurnal warming (cool-skin is only about a few millimeters thick, Fig. 4). Indeed we obtained a change in the OMB in the tropics, the most change, as shown in Fig. 10 was obtained in the Indian ocean (region is shown in inset), from morning to afternoon, thereafter our diurnal warming rapidly erodes and the background fit to these observations is almost the same as that for the OSTIA SST (standard deviation of OMB for our experiments and OSTIA SST was within 0.4^oK). This quick decay of our ΔT_w past sunset is expected to be addressed with the aid of a more realistic Stokes velocity (section 2.2), and also perhaps by following ZB05 when $Q^w_{net} \leq 0$; these topics will be addressed in future work.

Fig. 10 also shows that even though the spatial variation of the DSA shown in Fig. 9 for the Indian Ocean was large, yet the fit to the observations is improved (though we do not have observations everywhere). The spikes (less than -0.2^oC) in the fit background to observations on Apr 16 and 18 for Assim_Sol82 and Assim_PS81 are due to the larger background temperature obtained by the corresponding shortwave absorption profiles. The monthly averaged mean and standard deviations of the fit to the

[§]not all the drifter observations are used by OSTIA, since it is an analysis for a foundation SST, local daytime observations at low (< 6 m/s) wind speed are excluded; please see section 3 of (Donlon *et al.* 2012) for further details

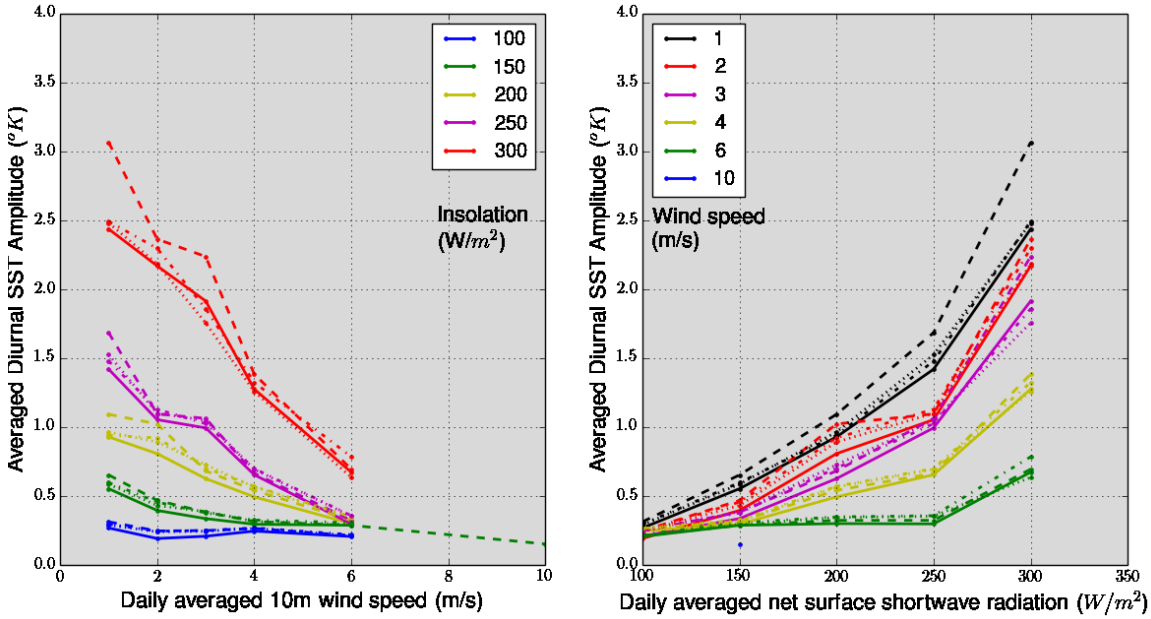

Figure 8. Averaged DSA (^oK) as a function of (left) 10m wind speed, and (right) insolation for Apr 2012; tSkin experiment is plotted with '-', Assim_Kpar ('- -'), Assim_Sol82 ('-.'), and Assim_PS81 (':'). Binning intervals for wind speed and insolation are 0.2 m/s and 10 W/m^2 respectively. Data is plotted only if sample size is > 100, average is over the experiment time period.

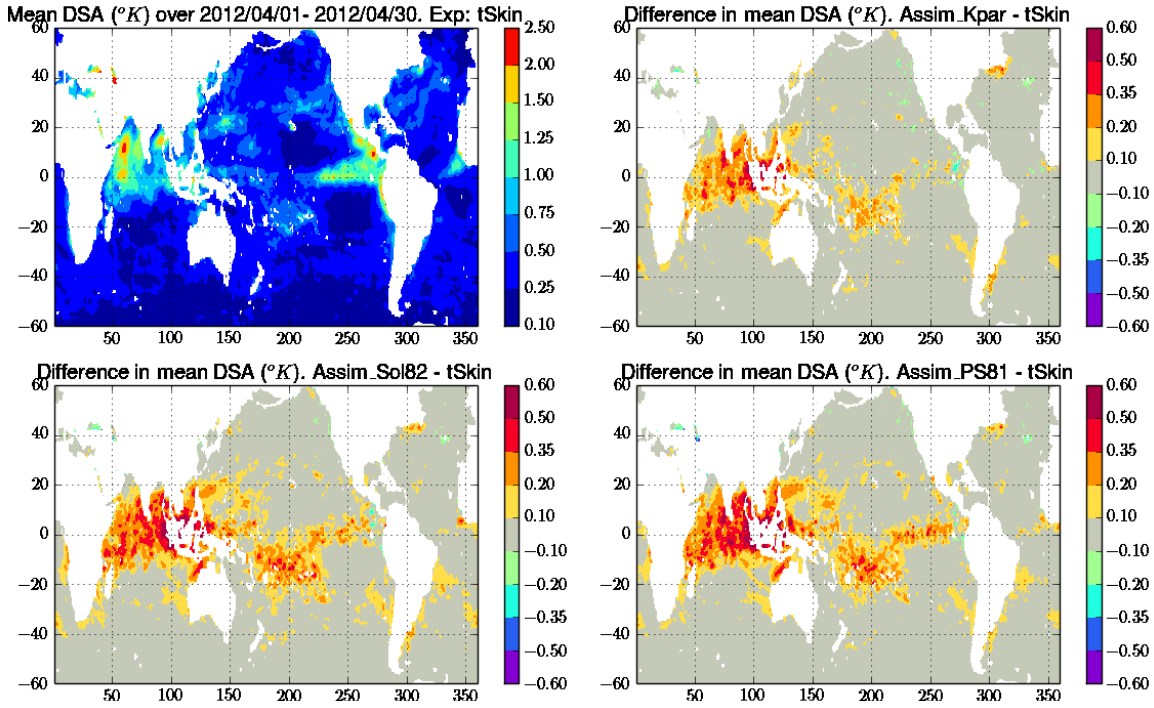

Figure 9. Spatial map of mean DSA (^oK). Top left panel is for tSkin experiment, all other panels depict differences for other experiments from it.

observations for the different experiments were very similar to each other and showed a small improvement compared to that for OSTIA SST. For example, in the tropical Indian ocean region (Fig. 10), the mean fit of background to observations for OSTIA SST is 0.145^oK, and for tSkin, Assim_Kpar, Assim_Sol82, Assim_PS81 it is $0.108^o, 0.095^o, 0.088^o, 0.089^oK$ respectively. The standard deviation changes by less than 2% (compared to that for OSTIA SST). Based on these differences between tSkin and T_s assimilation experiments, though the mean fit of background to observations for the assimilation experiments were slightly lower than tSkin (and OSTIA SST), we cannot conclude that the assimilation for T_s (and the ensuing air-sea fluxes) significantly improves the fit to these observations than what we obtained without it (as in tSkin). However, these results indicate that our implementation of the TBBJ10 diurnal warming is able to capture part of the diurnal cycle. We arrived at similar conclusions

based on evaluation with respect to the tropical moored buoys (TAO/TRITON, PIRATA, RAMA) measured SST at about 1 m. Our future work will be directed towards assimilating these observations and we hope to obtain better fit to these observations.

We added AVHRR (ocean only observations) to the analysis observing system (section 3.2), the AVH and T_s *assimilation experiments* assimilated these observations (Table 1). By comparing their AVHRR-OMB we try to assess the impact of skin SST model and T_s analysis versus using OSTIA SST. Fig. 11 shows the April 2012 monthly averaged OMB before any bias correction, for the surface sensitive channel 3 on Metop-A (supposed to measure brightness temperatures at about $15\mu m$ below the air-sea interface (11), i.e., in the cool-skin layer). There seems to be a positive impact of the skin SST, and in this case, the cool-skin (this channel is used only during night time when diurnal warming is almost absent), on the OMB as shown in Fig. 11, the T_s *assimilation experiments* have a reduced OMB in the tropics, southern hemisphere and also in the northern hemisphere high latitudes (north Pacific ocean).

Table 2 provides a summary of the OMB statistics for other AVHRR channels also on Metop-A. As shown in Fig. 11, for channel 3, AVH has a larger OMB before bias correction is applied, hence larger ($\sim 0.1^oK$) mean bias correction than the T_s *assimilation experiments*. For channels 4 and 5, we see a decrease in the OMB in the high latitudes which is offset by an increase in the tropics (not shown) thereby yielding a small increase in the mean bias correction for channel 4 and neutral for channel 5. Overall, for all the experiments the bias corrected mean OMB is close to zero and the standard deviations are below the specified observation error values.

We also obtained minor improvements to the analysis of other IR and MW sensors, that are currently being assimilated in GEOS-ADAS, suggesting a positive synergistic contribution from the skin SST model, assimilation of the AVHRR observations and usage of T_s analysis increment. For example, the OMB (before bias correction) for channel 123 of the atmospheric infrared sounder (AIRS) on the AQUA satellite (a surface sensitive window channel, measuring at about 11.8 micro-meters wavelength), for the CTL and AVH were alike. However, tSkin and T_s *assimilation experiments* have a reduced cold bias in the

Table 2. Comparison of mean OMB statistics (in ^oK) for the AVHRR observations on board Metop-A for the AVH and T_s *assimilation experiments*. Specified value of observational error standard deviation (SDEV) for each channel is given by σ_o. The average number of observations (Nobs), mean and SDEV of bias corrected OMB and mean bias correction are calculated using all the analyses within the experiment time period. Channel 3 is used during local nighttime only, hence the smaller number of observations than for channels 4 and 5.

Exp. Name	Nobs	Mean	SDEV	Mean Bias Corr
	Ch.3		σ_o =0.6^oK	
AVH	1054	-0.041	0.324	0.212
Assim_Kpar	1079	0.014	0.330	0.109
Assim_Sol82	1080	0.016	0.331	0.113
Assim_PS81	1080	0.015	0.330	0.109
	Ch.4		σ_o =0.68^oK	
AVH	2267	0.030	0.424	-0.041
Assim_Kpar	2314	0.048	0.429	-0.106
Assim_Sol82	2316	0.047	0.428	-0.106
Assim_PS81	2316	0.046	0.428	-0.108
	Ch.5		σ_o =0.72^oK	
AVH	2545	0.086	0.534	0.036
Assim_Kpar	2596	0.097	0.538	-0.014
Assim_Sol82	2599	0.097	0.538	-0.015
Assim_PS81	2597	0.095	0.537	-0.016

OMB in the southern oceans and northern Pacific (not shown; please see Akella *et al.* (2016)). Besides a small reduction in mean bias for these surface sensitive window channels, we also obtained a reduction in the standard deviation for the water vapor sensitive and lower troposphere peaking channels as well, as shown in Fig. 12 for the infrared atmospheric sounding interferometer (IASI) on Metop-A. For IASI, just as with AIRS, the reduction in standard deviation is larger for the Assim_Kpar and Assim_PS81 than the tSkin experiment, whereas AVH did not show any change from the CTL. For the Assim_Sol82 experiment, there is a decrease of about 0.1^oK in standard deviation for the water vapor and surface sensitive channels, and an increase of similar magnitude for the stratospheric and tropospheric (upper and lower) sensitive channels. Further studies that focus on the channels that peak at higher in altitude (stratosphere, troposphere) are required to investigate this behavior with the Soloviev (1982) shortwave absorption profile.

5.3. T_s Analysis Increments

Analysis increments provide observational feedback to the model trajectory through IAU (Bloom *et al.* 1996), and are available at synoptic times (Rienecker *et al.* (2008); section 3). The monthly averaged analysis increment (12 UTC analyses) in T_s is shown in Fig.13. These increments are fed back to the model

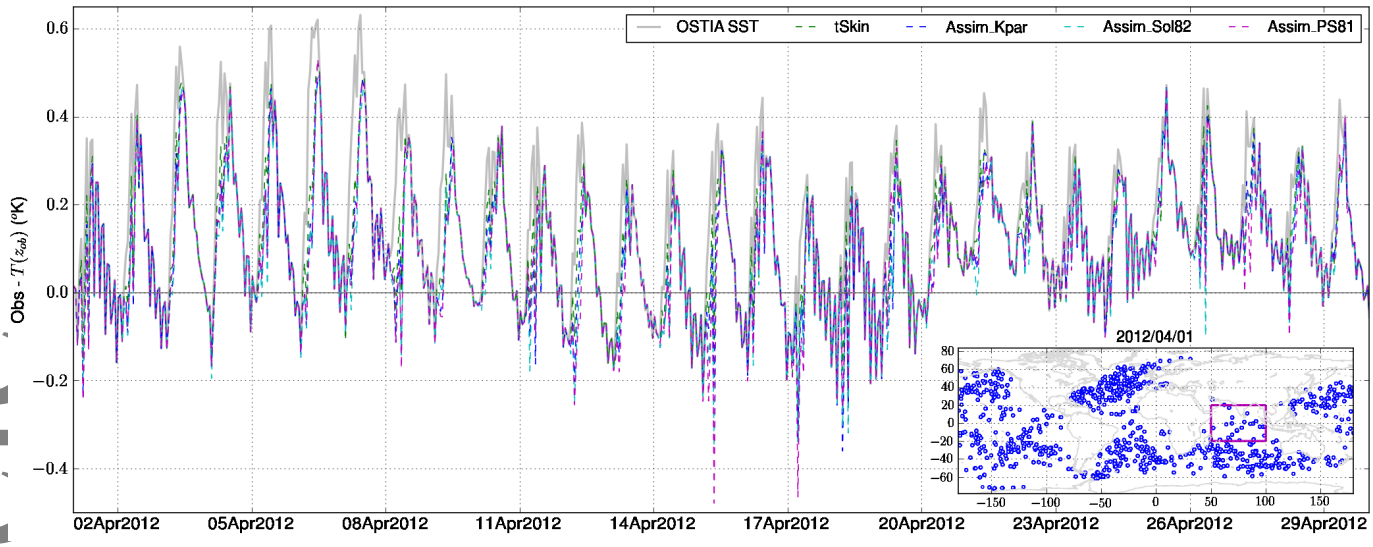

Figure 10. Time-series of hourly averaged differences between observed SST from drifting buoys and the temperature at 20cm depth from tSkin and T_s assimilation experiments for the tropical Indian ocean (20S-20N, 50E-100E) region shown in the inset. These observations were withheld from analysis, coverage on the Apr 1, 2012 is also shown in the inset plot. Time-series of observation minus OSTIA SST is also plotted in gray to show an estimate of the diurnal warming, assuming OSTIA SST to be foundation SST.

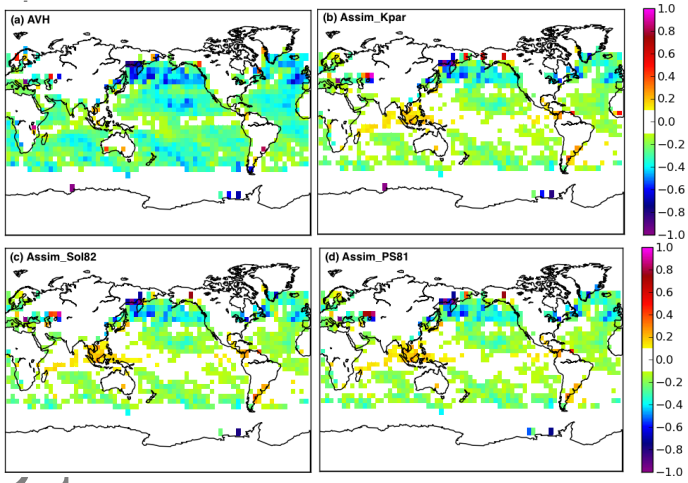

Figure 11. Monthly mean of the OMB (before bias correction, in ^oK) for channel 3 of the AVHRR on board Metop-A for (a) AVH, (b) Assim_Kpar, (c) Assim_Sol82, (d) Assim_PS81 experiments. This is a surface sensitive window channel, measuring at about 3.7 micro-meters wavelength, and was used only during local night time. The monthly mean has been computed by binning to $5^o \times 5^o$ uniform grid.

only in the T_s *assimilation experiments* (Table 1); for the other experiments, it serves merely as a diagnostic. Positive (negative) values of the increment indicate that the analyzed T_s is warmer (cooler) than the background (or, first guess) T_s; its spatial variation is related to the correlation length scales shown in Fig. 2. As Fig. 13 (a) and (b) indicate, there are small differences between CTL and AVH (e.g., Indian Ocean, western tropical Pacific Ocean) due to the assimilation of AVHRR observations in AVH. However, use of the skin SST model produces a larger difference in the increment, as evident by comparing Fig. 13 (a) and (c). Comparing the tSkin (Fig. 13(c)) and T_s *assimilation experiments* (Fig. 13(d)-(f)), there are differences due to the assimilation of AVHRR observations and feedback from the usage of the increment itself in the latter experiments. The averaged impact of the increment is to warm T_s in the eastern tropical Pacific by about 0.1^o K (local night time) and cool it by a similar amount in the Indian ocean Ocean (local day time). A similar pattern is seen in the increments for other analyses at $00, 16$ and 18 UTC. Overall, the increment for the T_s *assimilation experiments* is less biased than the CTL, AVH and tSkin experiments (for e.g., in the tropics: Indian Ocean). This suggests that the feedback lead to a more consistent ADAS when it comes to T_s than by not having the feedback active. The increments of other analyzed variables (surface pressure, atmospheric upper-air wind, temperature, moisture), show no significant differences among the different experiments.

6. Impact on predictions

Next, we assess how long the impact of the skin SST model, assimilation of AVHRR observations and use of T_s analysis increment, last in the self evaluation of five day forecasts, started from their corresponding 00UTC analyses. The forecast skill scores are calculated for 30 days in April 2012 and compared for global fields, not just over open water.

In the northern hemisphere extratropics (NHE) and the tropics, changes in the anomaly correlation (ACOR) and, also the root-mean-squared-errors (RMSE) were neutral. Whereas

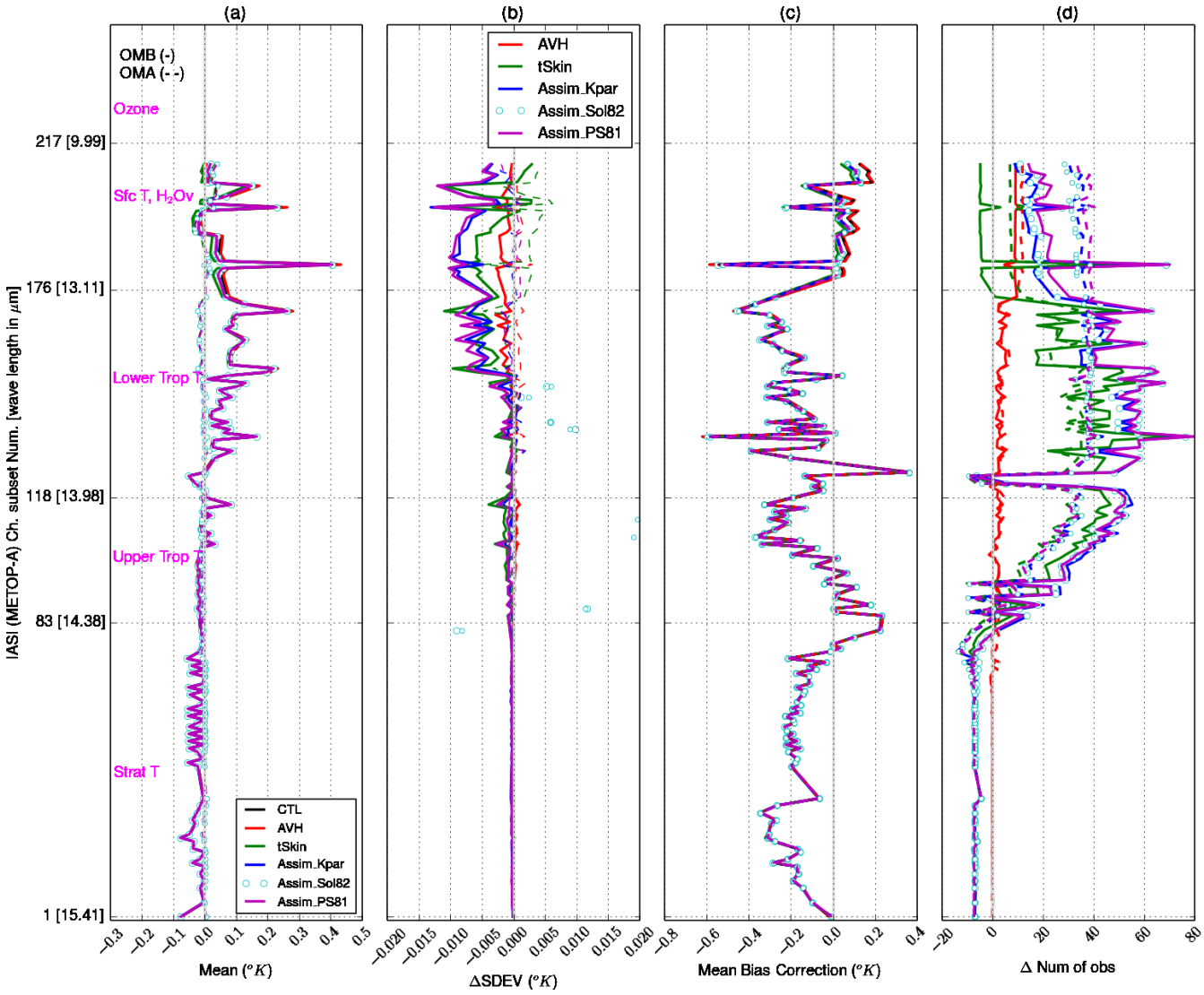

Figure 12. Monthly averaged OMB statistics for the the IASI on Metop-A satellite; statistics computed only over water. (left to right) Panels (a) and (c) show the mean bias corrected OMB and mean bias correction (defined in Table 2); (c) and (d) depict the difference (from CTL) in the bias corrected standard deviation (SDEV) of OMB and number of observations respectively. The ordinate is same for all panels, is shown in (a). Solid (dashed) lines are for OMB (OMA). Panel (a) shows the approximate regions of the atmosphere where channels *peak*.

in the southern hemisphere extratropics (SHE) forecasts from the Assim_Kpar have the highest ACOR, followed by other experiments. Figure 14 shows the ACOR for the SHE global geopotential height field at 850 hPa; skills for other variables were marginally better and any improvements in the skill diminished with increasing height.

7. Summary and conclusions

Skin SST is very important for air-sea interaction and in the GEOS-5 ADAS it is currently specified from an already existing daily OSTIA SST product. This prescription of the skin SST neglects a considerable variability in the diurnal cycle and the very thin cool skin layer in contact with the atmosphere, that is observed by radiometric and in situ observations taken close to the sea surface. The present work updates the GEOS-5 ADAS skin SST formulation by incorporating these effects in the model in an attempt to obtain a realistic evolution of T_s and focussed on its estimation by analysis and assimilation of near surface SST relevant observations.

A skin SST model was added to the air-sea interface component of the AGCM to prognostically compute: (i) a diurnal warming, mostly based on ZB05 and TBBJ10, and (ii) a diagnostic cool-skin layer following F96. Both of these effects are applied on top of the OSTIA SST, and the latter is taken as a foundation SST.

We adapt the TBBJ10 diurnal warming model, with the following three modifications. First, due to the absence of a wave model, we used a global constant value for the surface Stokes velocity. Second (due to the first reason), we chose not to follow the ZB05/TBBJ10 procedure to simulate the slow decay of diurnal warming in the late afternoon- evening local time. We

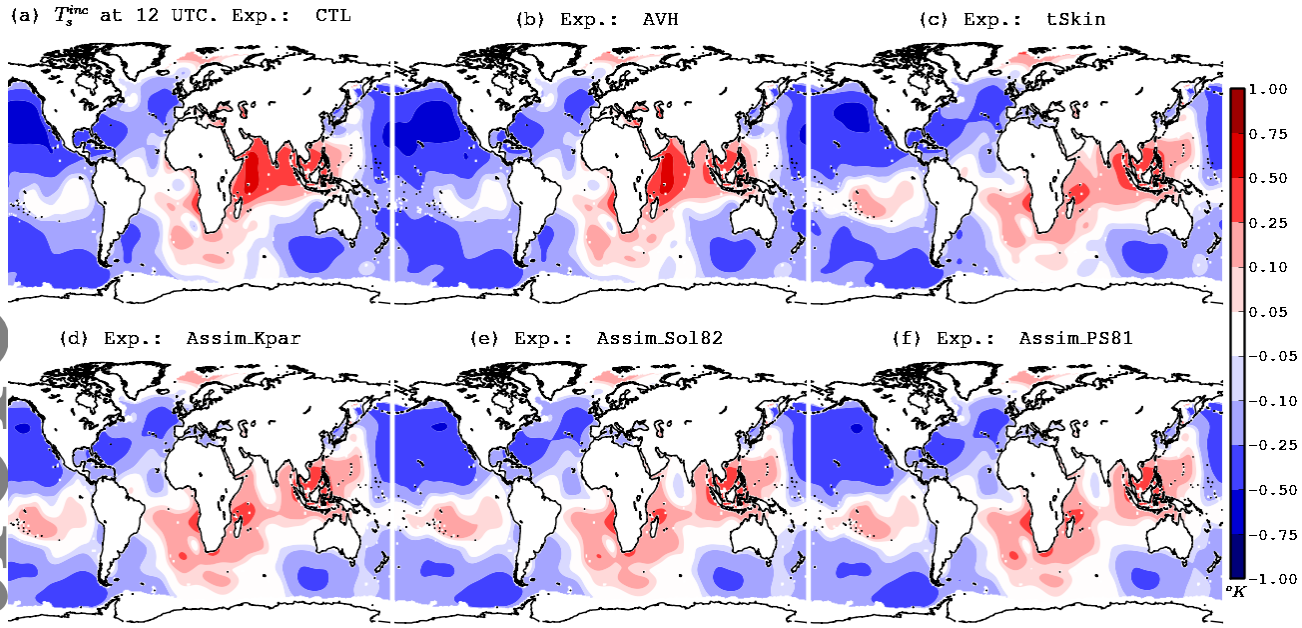

Figure 13. Monthly mean of the analysis increment in skin SST for the 12 UTC analyses; (a) CTL, (b) AVH, (c) tSkin, (d) Assim_Kpar, (e) Assim_Sol82, and (f) Assim_PS81 over open water (land and sea ice regions have been masked).

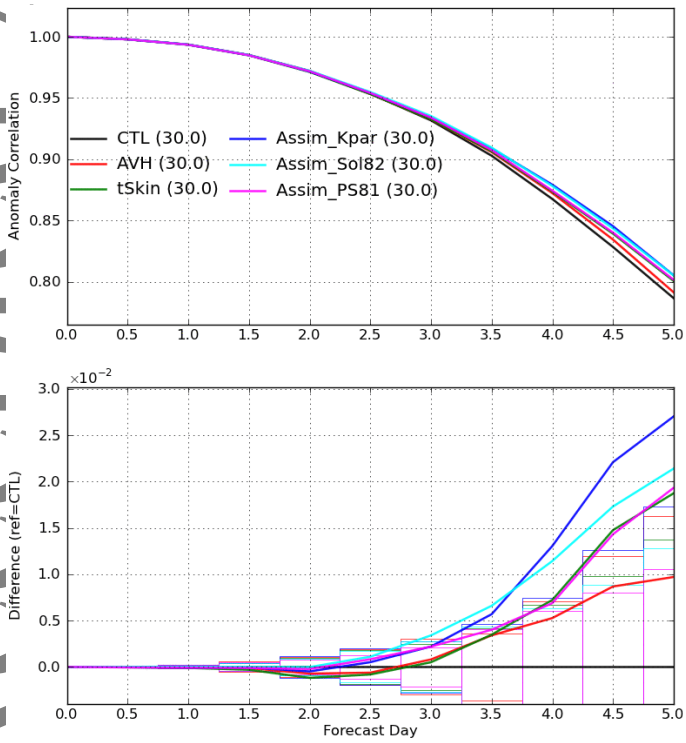

Figure 14. Top panel: anomaly correlation (ACOR) for souther hemisphere extratropics at 850-hPa geopotential height for five day forecasts from 00UTC analyses over April 2012. The numbers in the parenthesis denote the number of forecast samples used to calculate ACOR. Bottom panel: difference in ACOR between the experiments and CTL, bars denote 95% confidence intervals.

are concurrently working to incorporate a wave component in the GEOS-ADAS and plan to revisit this topics thereafter. Finally, in addition to the three band shortwave absorption model used by ZB05, and TBBJ10, our implementation of the shortwave absorption is flexible in exploring a model with nine bands and another that includes absorption in the visible and ultraviolet parts of the spectrum, making use of the photosynthetically active radiation (PAR) flux that changes light absorption characteristics of water based on water turbidity/biological activity. As a result, the ratio of absorbed to incident insolation is about $0.5 - 0.65$, as compared to a global constant of 0.61 obtained from the three band model.

The GSI atmospheric analysis includes the skin SST as a control variable when analyzing upper-air and surface pressure fields. However, the increment in T_s was simply ignored in the next forecast cycle of the AGCM.

Taking advantage of the existing analysis infrastructure, we made the following changes: (i) added the relevant diurnal output from the modified AGCM to compute a near-surface vertical thermal structure (that is, $T(z)$), (ii) use this $T(z)$ to compute first guess temperatures at (approximate) measurement depth, (iii) added SST relevant observations (AVHRR) to the observing system, and (iv) the increment in skin SST was fedback to the AGCM through the IAU component.

To test these updates to the model and analysis systems, we conducted several experiments and compared them to a control (CTL) which had none of these changes activated. The

AVH experiment was designed to test the impact of AVHRR observations only, tSkin tested the impact of the skin SST model only, and finally three T_s *assimilation experiments* combined all the updates (active skin SST model, AVHRR observations, and T_s analysis increment feedback to the AGCM); they differ only in the shortwave absorption models.

As a result of the cool skin layer model, the amount of cooling is inversely proportional to the wind speed, minimum and maximum values of cooling are about 0.05^o and 0.5^oK respectively. The diurnal variation in the net heat flux produce a maximum variability of about 0.2^oK in areas with large insolation and low wind speed (e.g., Indian Ocean). By comparing the tSkin and T_s *assimilation experiments*, we notice a very small impact (less than 0.02^oK) on cool skin layer. The maximum diurnal warming is about 2^oK in the tropical oceans and it is lower in the extratropics. The peak warming occurs about 2 to 3 hours after local noon time, which is similar to that obtained by ZB05, TBBJ10 and observations reported by F96. But due to the differences between our diurnal model implementation and TBBJ10 mentioned above, we obtain a quick erosion of our diurnal warming after sunset, indicating an excessive amount of dissipation. We also obtain a DSA of about $2.5^o - 3^oK$ at low wind speeds, as in ZB05, but about $0.5 - 1^oK$ more than TBBJ10. Considering figure 3 of TBBJ10, this may also be related to our simplification of the Stokes velocity; however, DSA is not directly measured and there are uncertainties in its estimation. Overall, the difference between skin and OSTIA SST is between -0.6^o to 1.5^oK. The difference between tSkin and T_s assimilation experiments was about 0.2^oK in the late afternoon to evening local times.

We evaluate the temperature within the diurnal warming layer by using withheld SST observations from drifting buoys. The fit to the observations is also compared with the observation-minus-OSTIA SST, because the latter is a foundation SST, hence serves as a reference. The calculated temperature is closer to the observations; in the tropics, particularly the Indian Ocean, where we obtain large diurnal warming, the morning to afternoon (rising part of the diurnal cycle) fit to the observations was lower than that for OSTIA SST. However, the late afternoon- evening part of the diurnal cycle does not show any improvement due to rapid erosion of our diurnal warming. Differences between tSkin and T_s *assimilation experiments* are small. Weaker diurnal cycle outside of the tropics lead to an insignificant change in the fit to the observations.

OMB statistics for satellite observations show a decrease in the mean bias with the usage of the skin SST model; there is a systematic improvement in the simulated brightness temperature. In particular, the OMB for hyperspectral IR instruments (AIRS and IASI) also reveals a positive feedback from the skin SST and combination of assimilating AVHRR and T_s increment. The fit to the surface as well as the water vapor sensitive channels is improved for both tSkin and T_s *assimilation experiments*, with more benefit in the latter experiments; changes are insignificant for the AVH experiment. Feedback of the analysis increment in skin SST to the AGCM led to lower increments in skin SST in the T_s *assimilation experiments*, perhaps indicates a more self-consistent ADAS. Since the T_s analysis is univariate, there was no noticeable difference in the analysis increments of other analyzed variables.

The impact on the predictability of the model is mostly neutral. Among our experiments, the combination of all changes and shortwave absorption that included turbidity via PAR flux (Assim_Kpar experiment) show the best forecast skill scores, up to 5-days lead time. Statistically significant improvements are obtained in the southern hemisphere, close to the surface and, the significance diminished with altitude.

In summary, we acknowledge some drawbacks such as the rapid erosion of diurnal warming just after dawn and high sensitivity to low wind speed, which will be addressed by future improvements. We also plan to evaluate the impact on air-sea fluxes and near-surface climatology in our future work. Overall, our diagnostics indicate that the range of our skin SST, its spatial distribution and diurnal variation are comparable to the values reported by F96, ZB05, and TBBJ10 and also seem to improve fit to observed in situ and satellite observations.

Using an ocean mixed layer model to resolve the SST diurnal cycle in the ECMWF operational system Takaya *et al.* (2010b) obtained improvements in 3- 5 days ACOR of temperature (at lower levels, for e.g., 1000, 850 hPa), but they were statistically insignificant, also they reported no difference

in 500 hPa geopotential height ACOR. Conclusions based on our results using GEOS-ADAS cannot be extrapolated to the performance of other systems, since our forecasts are self-verified. However, Takaya *et al.* (2010b) (on pp.27) stress the importance of coupling between SST and errors in air-sea fluxes. In that regard, modeling for the skin SST and direct assimilation SST relevant observations, offers an opportunity to explicitly account for SST errors, and air-sea interface fluxes; and that was exactly the goal of our T_s *assimilation experiments*, which show the most positive results among other experiments considered here.

This point is reinforced by the work of McLay *et al.* (2012) in the US Navy NOGAPS operational ADAS system, which included an SST diurnal cycle and perturbations for SST analyses (in an ensemble data assimilation framework), taking a step in the direction of explcitly accounting for synoptic-scale local SST variability. Based on forecasts up to lead times of 10 to 14 days they report statistically significant improvements in skin temperature (land and sea), 2-m air temperature, 10 m wind speed, 500 hPa geopotential heights and daily accumulated precipitation.

Taking into consideration results of Takaya *et al.* (2010b); McLay *et al.* (2012) and ours (in GEOS-ADAS), incorporating related modifications to the SST, mostly lead to positive improvements in the forecasts. Further revisit of skin SST modeling, air-sea fluxes, coupling with a wave model, tuning of atmospheric boundary layers, modeling of the observational and background errors (using ensemble methods) should be pursed along with the incorporation of MW and in situ SST observations in the context of the development of a coupled data assimilation system.

Acknowledgement

This work was partially funded by NASA ROSES 2010, NNH10ZDA001N-MAP. We thank Michele Rienecker for her initial guidance. Xu Li and John Derber are thanked for sharing their initial development within the GSI. We thank Chelle Gentemann for helpful suggestions and diagnostics performed on our diurnal warming model, Xubin Zeng and Anton Beljaars for sharing their diurnal model and helping with evaluation of results. We thank F. Xu and Alex Ignatov for making the iQuam data set publicly available. Thanks are also due to Will McCarty and Meta Sienkiewicz for their help with satellite bias correction and radiative transfer; Lawrence Takacs for help with the forecast verification and Chris Fairall for suggestions on the bulk to skin temperature modeling. Computations were performed at NASA NCCS.

References

Akella S, Todling R, Suarez M. 2016. Estimation of the ocean skin temperature using the NASA GEOS Atmospheric Data Assimilation System. Technical Report Series on Global Modeling and Data Assimilation NASA/TM-2016-104606/Vol 44, NASA Goddard Space Flight Center.

Beljaars ACM. 1997. Air-sea interaction in the ECMWF model. Seminar on Atmosphere-Surface Interactions. ECMWF, Reading, U. K.

Bellenger H, Duvel JP. 2009. An analysis of tropical ocean diurnal warm layers. *J. Climate* **22**: 3629– 3646, doi:10.1175/2008JCLI2598.1.

Bloom SC, Takacs LL, da Silva AM, Ledvina D. 1996. Data assimilation using incremental analysis updates. *Mon Weather Rev* **124**: 1256–1271.

Bosilovich MG, Akella S, Coy L, Cullather R, Draper C, Gelaro R, Kovach R, Liu Q, Molod A, Norris P, Wargan K, Chao W, Reichle R, Takacs L, Vikhliaev Y, Bloom S, Collow A, Firth S, Labow G, Partyka G, Pawson S, Reale O, Schubert SD, Suarez M. 2015. MERRA-2: Initial evaluation of the climate. Technical Report Series on Global Modeling and Data Assimilation NASA/TM-2015-104606/Vol 43, NASA Goddard Space Flight Center.

Brassington GB, Martin MJ, Tolman HL, Akella S, Balmeseda M, Chambers CRS, Chassignet E, Cummings JA, Drillet Y, Jansen PAEM, Laloyaux P, Lea D, Mehra A, Mirouze I, Ritchie H, Samson G, Sandery PA, Smith GC, Suarez M, Todling R. 2015. Progress and challenges in short- to medium-range coupled prediction. *J Operational Oceanography.* **8**: s239– s258, doi: 10.1080/1755876X.2015.1049875.

Brunke MA, Zeng X, Misra V, Beljaars A. 2008. Integration of a prognostic sea surface skin temperature scheme into weather and climate models. *J Geophys Res-Atmos* **113**: D21 117, doi: 10.1029/2008JD010607.

Castro SL, Wick GA, Emery WJ. 2012. Evaluation of the relative performance of sea surface temperature measurements from different types of drifting and moored buoys using satellite-derived reference products. *J Geophys Res-Oceans* **117**: C02 029, doi:10.1029/2011JC007472.

Castro SL, Wick GA, Jackson DL, Emery WJ. 2008. Error characterization of infrared and microwave satellite sea surface temperature products for merging and analysis. *J Geophys Res* **113**: C03 010, doi:10.1029/2006JC003829.

Chen Y, Han Y, Delst PV, Weng F. 2010. On water vapor Jacobian in fast radiative transfer model. *J Geophys Res* **115**: D12 303, doi:10.1029/2009JD013379.

Chen Y, Han Y, Weng F. 2012. Comparison of two transmittance algorithms in the community radiative transfer model: Application to AVHRR. *J Geophys Res-Atmos* **117**: D06 206, doi:10.1029/2011JD016656.

Curry JA, Bentamy A, Bourassa MA, Bourras D, Bradley EF, Brunke M, Castro S, Chou SH, Clayson CA, Emery WJ, Eymard L, Fairall CW, Kubota M, Lin B, Perrie W, Reeder RA, Renfrew IA, Rossow WB, Rossow WB, Schulz J, Smith SR, Webster PJ, Wick GA, Zeng X. 2004. Seaflux. *Bull. Amer. Meteor. Soc.* **85**: 409–424, doi:http://dx.doi.org/10.1175/BAMS-85-3-409.

Dee D, Uppala S. 2009. Variational bias correction of satellite radiance data in the ERA-interim reanalysis. *Q. J. R. Meteorol. Soc.* **135**: 1830– 1841, doi:10.1002/qj.493.

Dee DP, Balmaseda M, Balsamo G, Engelen R, Simmons AJ, Thépaut JN. 2014. Toward a consistent reanalysis of the climate system. *Bull. Amer. Meteor. Soc.* **95**: 1235–1248, doi:http://dx.doi.org/10.1175/BAMS-D-13-00043.1.

Derber JC, Wu WS. 1998. The use of TOVS Cloud-Cleared Radiances in the NCEP SSI analysis system. *Mon Weather Rev* **126**: 2287– 2299, doi:http://dx.doi.org/10.1175/1520-0493(1998)126⟨2287:TUOTCC⟩2.0.CO;2.

Donlon C, Minnett PJ, Gentemann C, Nightingale TJ, Barton IJ, Ward B, Murray MJ. 2002. Toward improved validation of satellite sea surface skin temperature measurements for climate research. *J. Climate* **15**: 353–369.

Donlon C, Robinson I, Casey KS, Vazquez-Ciervo J, Armstrong E, Arino O, Gentemann C, May D, Le Borgne P, Piollé J, Barton I, Beggs H, Poulter DJS, Merchant CJ, Bingham A, Heinz S, Harris A, Wick G, Emery B, Minnett P, Evans R, Llewellyn-Jones D, Mutlow C, Reynolds RW, Kawamura H, Rayner N. 2007. The global ocean data assimilation experiment high-resolution sea surface temperature pilot project. *Bull. Amer. Meteor. Soc* **88**: 1197–1213, doi:http://dx.doi.org/10.1175/BAMS-88-8-1197.

Donlon CJ, Martin M, Stark J, Roberts-Jones J, Fiedler E, Wimmer W. 2012. The Operational Sea Surface Temperature and Sea Ice Analysis (OSTIA) system. *Remote Sens. Environ.* **116**: 140–158, doi:10.1016/j.rse.2010.10.017.

Eyre JR. 2016. Observation bias correction schemes in data assimilation systems: a theoretical study of some of their properties. *Q. J. R. Meteorol. Soc.* **142**: 2284– 2291, doi:10.1002/qj.2819.

Fairall CW, Bradley EF, Godfrey JS, Wick GA, Edson JB, Young GS. 1996. Cool-skin and warm-layer effects on sea surface temperature. *J Geophys Res-Oceans* **101**: 1295–1308, doi:10.1029/95JC03190.

Filipiak MJ, Merchant CJ, Kettle H, Borgne PL. 2010. A statistical model for sea surface diurnal warming driven by numerical weather prediction fluxes and winds. *Ocean Sci. Discuss.* **7**: 1497–1532, doi:10.5194/osd-7-1497-2010.

Gentemann CL, Donlon CJ, Stuart-Menteth A, Wentz FJ. 2003. Diurnal signals in satellite sea surface temperature measurements. *Geophys. Res. Lett.* **30**: 1140, doi:10.1029/2002GL016291.

Gentemann CL, Minnett PJ. 2008. Radiometric measurements of ocean surface thermal variability. *J. Geophys. Res.* **113**: C08 017, doi:10.1029/2007JC004540.

Gentemann CL, Minnett PJ, Ward B. 2009. Profiles of ocean surface heating (POSH): A new model of upper ocean diurnal warming. *J. Geophys. Res.* **114**: C07 017, doi:10.1029/2008JC004825.

Ham YG, Rienecker MM, Suarez MJ, Vikhliaev Y, Zhao B, Marshak J, Vernieres G, Schubert SD. 2014. Decadal prediction

skill in the GEOS-5 forecast system. *Clim Dyn* **42**: 1–20, doi: 10.1007/s00382-013-1858-x.

Han Y, van Delst P, Liu Q, Weng F, Yan B, Treadon R, Derber J. 2006. JCSDA Community Radiative Transfer Model (CRTM)-version 1. NOAA Technical Report NESDIS 122, U.S. Dept of Commerce, NOAA, Washington, D.C.

Hosoda K. 2010. A review of satellite-based microwave observations of Sea Surface Temperatures. *J Oceanogr* **66**: 439–473.

Kawai Y, Wada A. 2007. Diurnal Sea Surface Temperature variation and its impact on the Atmosphere and Ocean: A Review. *J Oceanogr* **63**: 721–744.

Kennedy JJ, Brohan P, Tett SFB. 2007. A global climatology of the diurnal variations in sea-surface temperature and implications for MSU temperature trends. *Geophys. Res. Lett.* **34**: L05 712, doi:10.1029/2006GL028920.

Kleist DT, Parrish DF, Derber JC, Treadon R, Errico RM, Yang R. 2009a. Improving incremental balance in the GSI 3DVAR analysis system. *Mon Weather Rev* **137**: 1046–1060, doi:10.1175/2008MWR2623.1.

Kleist DT, Parrish DF, Derber JC, Treadon R, Wu WS, Lord S. 2009b. Introduction of the GSI into the NCEP Global Data Assimilation System. *Wea. Forecasting* **24**: 1691–1705, doi: http://dx.doi.org/10.1175/2009WAF2222201.1.

Laloyaux P, Balmaseda MA, Dee D, Mogensen K, Janssen P. 2016a. A coupled data assimilation system for climate reanalysis. *Q. J. R. Meteorol. Soc.* **142**: 65– 78, doi:10.1002/qj.2629.

Laloyaux P, Thépaut JN, Dee D. 2016b. Impact of scatterometer surface wind data in the ECMWF coupled assimilation system. *Mon Weather Rev* **144**: 1203– 1217, doi:http://dx.doi.org/10.1175/MWR-D-15-0084.1.

Lea DJ, Mirouze I, Martin MJ, King RR, Hines A, Walters D, Thurlow M. 2015. Assessing a new coupled data assimilation system based on the Met Office coupled atmosphere–land–ocean–sea ice model. *Mon Weather Rev* **143**: 4678– 4694, doi: http://dx.doi.org/10.1175/MWR-D-15-0174.1.

Liang XM, Ignatov A, Kihali Y. 2009. Implementation of the Community Radiative Transfer Model in Advanced Clear-Sky Processor for oceans and validation against nighttime AVHRR radiances. *J. Geophys. Res.* **114**: D06 112, doi:10.1029/2008JD010960.

Lumpkin R, Pazos M. 2007. *Measuring surface currents with surface velocity program drifters: The instrument, its data and some results.*, ch. 2. Lagrangian Analysis and Prediction of Coastal and Ocean Dynamics (LAPCOD), Cambridge University Press, pp. 39– 67, doi:http://dx.doi.org/10.1017/CBO9780511535901.003.

May DA, Parmeter MM, Olszewski DS, McKenzie BD. 1998. Operational processing of Satellite Sea Surface Temperature retrievals at the Naval Oceanographic Office. *Bull. Amer. Meteor. Soc.* **79**: 397– 407, doi:http://dx.doi.org/10.1175/1520-0477(1998)079⟨0397:OPOSSS⟩2.0.CO;2.

May DA, Stowe LL, Hawkins JD, McClain EP. 1992. A correlation of Saharan dust effects on satellite sea surface temperature measurements. *J Geophys Res* **97**: 3611– 3619.

McLay JG, Flatau MK, Reynolds CA, Cummings J, Hogan T, Flatau PJ. 2012. Inclusion of sea-surface temperature variation in the U.S. Navy ensemble-transform global ensemble prediction system. *J. Geophys. Res.* **117**: D19 120, doi:10.1029/2011JD016937.

Merchant CJ, Embury O, Le Borgne P, Bellec B. 2006. Saharan dust in nighttime thermal imagery: Detection and reduction of related biases in retrieved sea surface temperature. *Remote Sens. Environ.* **104**: 15– 30, doi:10.1016/j.rse.2006.03.007.

Molod A, Takacs L, Suarez M, Bacmeister J, Song IS, Eichmann A. 2012. The GEOS-5 Atmospheric General Circulation Model: Mean Climate and Development from MERRA to Fortuna. Technical Report Series on Global Modeling and Data Assimilation NASA/TM-2012-104606/Vol 28, NASA Goddard Space Flight Center.

Morel A, Huot Y, Gentili B, Werdell PJ, Hooker SB, Franz BA. 2007. Examining the consistency of products derived from various ocean color sensors in open ocean (Case 1) waters in the perspective of a multi-sensor approach. *Remote Sens. Environ.* **111**: 69– 88, doi:10.1016/j.rse.2007.03.012.

Ohlmann JC. 2003. Ocean radiant heating in climate models. *J. Climate* **16**: 1337– 1351, doi:http://dx.doi.org/10.1175/1520-0442-16.9.1337.

Ohlmann JC, Siegel DA. 2000. Ocean radiant heating. Part II: Paramterizing solar radiation transmission through the upper ocean. *J Phys Oceanogr* **30**: 1849–1865.

Paulson CA, Simpson JJ. 1981. The temperature difference across the cool skin of the ocean. *J. Geophys. Res.* **86(C11)**, doi:10.1029/JC086iC11p11044.

Putman WM, Lin SJ. 2007. Finite-volume transport on various cubed-sphere grids. *J Comput Phys* **227**: 55– 78, doi:10.1016/j.jcp.2007.07.022.

Reynolds RW, Rayner NA, Smith TM, Stokes DC, Wang Q. 2002. An improved in situ and satellite SST analysis for climate. *J. Climate* **15**: 1609–1625.

Reynolds RW, Smith TM, Liu C, Chelton DB, Casey KS, Schlax MG. 2007. Daily high-resolution-blended analyses for Sea Surface Temperature. *J. Climate* **20**: 5473–5496, doi:10.1175/2007JCLI1824.1.

Rienecker MM, Suarez M, Todling R, Bacmeister J, Takacs L, Liu HC, Gu W, Sienkiewicz M, Koster RD, Gelaro R, Stajner I, Nielsen JE. 2008. The GEOS-5 Data Assimilation System. Documentation of versions 5.0.1 and 5.1.0, and 5.2.0. Technical Report Series on Global Modeling and Data Assimilation NASA/TM-2008-104606/Vol 27, NASA Goddard Space Flight Center.

Rienecker MM, Suarez MJ, Gelaro R, Todling R, Bacmeister J, Liu E, Bosilovich MG, Schubert SD, Takacs L, Kim GK, Bloom S, Chen J, Collins D, Conaty A, da Silva A, Gu W, Joiner J, Koster RD, Lucchesi R, Molod A, Owens T, Pawson S, Pegion P, Redder C, Reichle R, Robertson FR, Ruddick AG, Sienkiewicz M, Woollen J. 2011. MERRA: NASAs Modern-Era Retrospective Analysis for Research and Applications. *J. Climate* **24**: 3624–3648, doi:10.1175/JCLI-D-11-00015.1.

Saunders PM. 1967. The Temperature at the Ocean-Air Interface. *J Atmos Sci* **24**: 269–273.

Soloviev A, Lukas R. 1997. Observation of large diurnal warming events in the near-surface layer of the western equatorial Pacific warm pool. *Deep-Sea Res* **44**: 1055–1076.

Soloviev AV. 1982. On the vertical structure of the ocean thin surface layer at light wind. *Dokl. Acad. Sci. USSR Earth Sci. Sect. Engl. Transl.* **18**: 751–760.

Takaya Y, Bidlot JR, Beljaars ACM, Janssen PAEM. 2010a. Refinements to a prognostic scheme of skin sea surface temperature. *J Geophys Res-Oceans* **115**: C06 009, doi:10.1029/2009JC005985.

Takaya Y, Vitart F, Balsamo G, Balmaseda M, Leutbecher M, Molteni F. 2010b. Implementation of an ocean mixed layer model in IFS. Technical Memorandum 622, European Centre for Medium-Range Weather Forecasts, Shinfield Park, Reading, RG2 9AX, England, URL http://www.ecmwf.int/publications/.

Vernieres G, Rienecker MM, Kovach R, Keppenne CL. 2012. The GEOS-iODAS: Description and Evaluation. Technical Report Series on Global Modeling and Data Assimilation NASA/TM-2012-104606/Vol 30, NASA Goddard Space Flight Center.

Ward B. 2006. Near-surface ocean temperature. *J. Geophys. Res.* **111**: C02 004, doi:10.1029/2004JC002689.

Webster PJ, Clayson CA, Curry JA. 1996. Clouds, radiation and the diurnal cycle of sea surface temperature in the tropical western Pacific. *J. Climate* **9**: 1712– 1730, doi:http://dx.doi.org/10.1175/1520-0442(1996)009⟨1712:CRATDC⟩2.0.CO;2.

While J, Martin M. 2013. Development of a variational data assimilation system for the diurnal cycle of sea surface temperature. *J Geophys Res-Oceans* **118**: 2845–2862, doi:doi:10.1002/jgrc.20215.

Wick GA, Ohlmann JC, Fairall CW, Jessup AT. 2005. Improved oceanic cool-skin corrections using a refined solar penetration model. *J Phys Oceanogr* **35**: 1986–1996.

Wieliczka DM, Weng S, Querry MR. 1989. Wedge shaped cell for highly absorbent liquids: infrared optical constants of water. *Appl Optics* **28**: 1714– 1719.

Xu F, Ignatov A. 2014. In situ SST Quality Monitor (iQuam). *J. Atmos. Oceanic Technol.* **31**: 164– 180, doi:http://dx.doi.org/10.1175/JTECH-D-13-00121.1.

Zeng X, Beljaars A. 2005. A prognostic scheme of sea surface skin temperature for modeling and data assimilation. *Geophys Res Lett* **32**(14): L14 605, doi:10.1029/2005GL023030.